and the three-"fluked" tail of *Odaraia* (*26*), are strictly unique. And a number involve the structure of the limbs, or the tail, features which may be functionally diverse even among closely related arthropods.

The PAUP analysis provides an additional measure of morphological separation, by the calibration of distances on the cladogram in terms of changes in coded character states. This shows that *Olenoides* and *Limulus*, bona fide trilobite and chelicerate, respectively, are the taxa furthest from the origin of the cladogram. This is hardly surprising as they are members of the most derived groups in the analysis, but it does emphasize that the problematic Cambrian taxa do not show any remarkable morphological separation. This leads to the expectation that the addition of further taxa (either later Paleozoic examples, or new Cambrian discoveries) would narrow rather than widen the morphological gaps between them.

The arrangement of taxa on the cladogram raises the possibility that the living crustaceans are a paraphyletic group. Analyses of the Recent crustaceans have emphasized that "aside from the features of the head, it is impossible to characterize crustaceans except by noting tendencies toward certain conditions or states" (*19, 21,* p. 3). The cladistic analysis of the Cambrian arthropods shows that the features of the head are poorly developed and that other criteria are more useful in identifying groupings. Thus the characters used to diagnose living crustaceans may be primitive or convergently acquired.

The significance of Cambrian problematica in formulating hypotheses of relationship has been largely ignored [the echinoderms are a notable exception (*27*)], or they have been simply set aside as groups of independent origin, thus obscuring their importance in phylogenetic analysis. The somewhat counterintuitive results of this analysis illustrate how critical the evidence of well-preserved fossils can be to understanding the affinities of living groups (*28*).

REFERENCES AND NOTES

1. J. L. Cisne, *Science* **186**, 13 (1974).
2. S. M. Manton, *The Arthropoda, Habits, Functional Morphology and Evolution* (Clarendon, Oxford, 1977).
3. C. Patterson, *Antenna* **2**, 99 (1978).
4. R. R. Hessler and W. A. Newman, *Fossils Strata* **4**, 437 (1975).
5. K.-E. Lauterbach, *Abh. Verh. Naturwiss. Ver. Hamburg* **23**, 163 (1980).
6. D. E. G. Briggs and S. Conway Morris, in *Problematic Fossil Taxa*, A. Hoffman and M. H. Nitecki, Eds. (Oxford Univ. Press, Oxford, 1986), pp. 167–183.
7. D. E. G. Briggs, in *Crustacean Phylogeny*, F. R. Schram, Ed. (Balkema, Rotterdam, 1983), pp. 1–22; *Recherche* **16**, 340 (1985).
8. L. Størmer, *Skr. Nor. Vidensk. Alkad. Oslo.* **5**, 1 (1944).
9. ———, in *Treatise on Invertebrate Paleontology*, part O, Arthropoda 1, R. C. Moore, Ed. (Geological Society of America and University of Kansas, Lawrence, KS, 1959), pp. 23–37.
10. D. T. Anderson, *Embryology and Phylogeny of Annelids and Arthropods* (Pergamon, Oxford, 1973).
11. S. M. Manton and D. T. Anderson, in *The Origin of Major Invertebrate Groups*, M. R. House, Ed. (Systematics Association, London, 1979), pp. 269–321; H. B. Whittington, *ibid.*, pp. 253—268.
12. D. E. G. Briggs and D. Collins, *Palaeontology* **31**, 779 (1988).
13. K. J. Müller and D. Walossek, *Fossils Strata* **19**, 1 (1987); *Zool. Scr.* **15**, 92 (1986); *Fossils Strata* **17**, 1 (1985).
14. D. E. G. Briggs *et al.*, *Palaeontology* **22**, 167 (1979).
15. H. L. Sanders, *Syst. Zool.* **6**, 112 (1957); F. R. Schram, in *Crustacean Phylogeny*, F. R. Schram, Ed. (Balkema, Rotterdam, 1983), pp. 23–28.
16. J. L. Cisne, *Paleontogr. Am.* **9**, 99 (1981); H. B. Whittington and J. E. Almond, *Philos. Trans. R. Soc. London Ser. B* **317**, 1 (1987).
17. P. A. Selden, *Trans. R. Soc. Edinburgh Earth Sci.* **72**, 9 (1981).
18. The data matrix and details of the methodology are given in D. E. G. Briggs and R. A. Fortey, in *Origins and Early Evolutionary History of the Metazoa*, J. H. Lipps and P. W. Signor, Eds. (Plenum, New York, in press).
19. D. E. G. Briggs and H. B. Whittington, in *Short Papers for the Second International Symposium on the Cambrian System*, M. E. Taylor, Ed. (Open-File Report 81-743, U.S. Geological Survey, Washington, D.C., 1981), pp. 38–41.
20. J. L. Cisne, in *The Biology of Crustacea*, D. E. Bliss, Ed. (Academic Press, New York, 1982), vol. 1, pp. 65–92.
21. F. R. Schram, *Crustacea* (Oxford Univ. Press, Oxford, 1986).
22. D. E. G. Briggs, *Philos. Trans. R. Soc. London Ser. B* **281**, 439 (1978).
23. H. B. Whittington, *Bull. Geol. Surv. Can.* **209**, 1 (1971).
24. ———, *Proc. Geol. Assoc.* **91**, 127 (1980); in *Palaeontology, Essential of Historical Geology*, E. M. Gallitelli, Ed. (S.T.E.M. Mucchi, Modena, 1982), pp. 11–24.
25. D. L. Bruton and H. B. Whittington, *Philos. Trans. R. Soc. London Ser. B* **300**, 553 (1983).
26. D. E. G. Briggs, *ibid.* **291**, 541 (1981).
27. A. B. Smith, *Palaeontology* **27**, 431 (1984); C. R. C. Paul and A. B. Smith, *Biol. Rev.* **59**, 443 (1984).
28. See J. Gauthier, A. G. Kluge, T. Rowe, *Cladistics* **4**, 105 (1988) for a tetrapod example.

29. We thank P. L. Forey for running the PAUP program and for discussion of the method and results. P. Baldaro drew the figure.

9 May 1989; accepted 23 August 1989

Detection of Cell-Affecting Agents with a Silicon Biosensor

J. WALLACE PARCE,* JOHN C. OWICKI, KAREN M. KERCSO, GEORGE B. SIGAL, H. G. WADA, VICTORIA C. MUIR, LUC J. BOUSSE, KEVIN L. ROSS, BRANIMIR I. SIKIC, HARDEN M. MCCONNELL

Cellular metabolism is affected by many factors in a cell's environment. Given a sufficiently sensitive method for measuring cellular metabolic rates, it should be possible to detect a wide variety of chemical and physical stimuli. A biosensor has been constructed in which living cells are confined to a flow chamber in which a potentiometric sensor continually measures the rate of production of acidic metabolites. Exploratory studies demonstrate several applications of the device in basic science and technology.

CHANGES IN THE BIOLOGICAL, chemical, and physical environment of a cell must be reflected in the concentrations and fluxes of molecules within the cell. The extensive interconnections among different biochemical processes assure that changes ripple outward from primary sites of action, and a sufficiently sensitive analytical method might detect a response in cellular characteristics not normally associated with the primary stimulus. The integrative role of catabolism makes it an excellent candidate for the indirect detection of responses.

We have constructed an instrument, which we have named a silicon microphysiometer, to investigate these phenomena. We report that ligand-receptor interactions can produce prompt changes in cellular catabolic rates. In addition, we find that cytotoxic and cytopathic effects can be detected. The physiological basis of the device is the acidity of the principal catabolic products in mammalian cells, lactate and CO_2. The acidity of the culture medium bathing a small sample of cells can be determined with a light-addressable potentiometric sensor (LAPS) (*1*), and the rate of acidification is used as a measure of catabolic rate.

The LAPS device configured as a biosensor is shown in Fig. 1. In the flow chamber the silicon forms the bottom wall of a fluid channel that is rectangular in cross section. The top wall of the fluid channel is formed by a glass cover slip that is coated on the channel side with a transparent conductive layer of indium–tin oxide. Typical channel

J. W. Parce, J. C. Owicki, K. M. Kercso, G. B. Sigal, H. G. Wada, V. C. Muir, L. J. Bousse, Molecular Devices Corporation, 4700 Bohannon Drive, Menlo Park, CA 94025.
K. L. Ross and B. I. Sikic, Stanford University School of Medicine (Oncology Division), Stanford, CA 94305.
H. M. McConnell, Chemistry Department, Stanford University, Stanford, CA 94305.

*To whom correspondence should be addressed.

dimensions are ~100 μm high, ~5 mm wide, and ~20mm long (volume ~10 μl).

The method for retaining cells in the flow chamber depends on the adherence properties of the cells. Adherent cells are simply grown on the glass cover slip before assembly of the chamber. Most adherent cells attach securely enough to resist the shear stresses of medium flow, but nonadherent cells are swept out of the chamber. Many methods have been developed to immobilize nonadherent cells (*2*), but we require a convenient technique that is applicable to the micrometer thickness scale and avoids the likely physiological perturbations of filtration (shear stress) or attachment to a surface via lectins or antibodies.

Our immobilization method involves micromachining the surface of the silicon sensor (Fig. 1 and cover). Cells sediment gravitationally into a 1-mm^2 array of wells etched into the surface of the sensor, each approximately 50 μm square and 50 μm deep with 25-μm-thick walls. Several layers of cells can be trapped by halting the flow of a suspension of ~10^8 cells per milliliter above the wells for ~1 min, then washing untrapped cells away at flow velocities of 10 to 50 μm per second. At these flow rates cells are not washed out of the wells. However, at much higher velocities the cells are removed from the wells, providing a means of loading, testing, flushing, and reloading cells for subsequent tests (*3*).

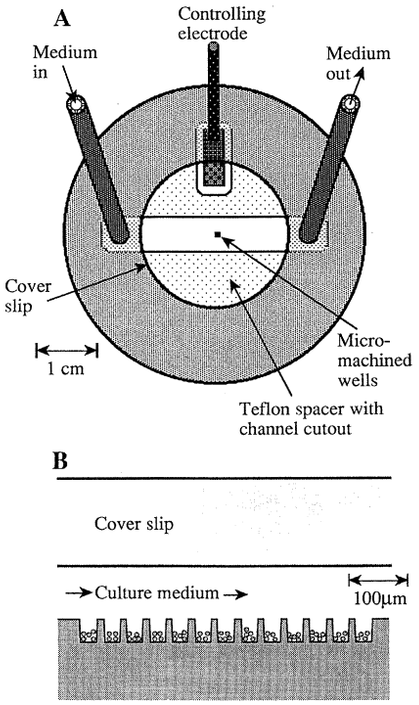

Fig. 1. Schematic view of the flow chamber. (**A**) Top view. (**B**) Vertical section through the center of the chamber along the flow path. The ohmic connection to the base of the LAPS is not shown, nor is the source of illumination (laser light from above the sensor or optic fiber from below).

With adherent cells, unpatterned silicon surfaces are used, fabricated as reported by Hafeman *et al.* (*1*), by first growing a thin (30 nm) thermal SiO_2 film, followed by a deposition of 100 nm of Si_3N_4 by low-pressure chemical vapor deposition. The first step in the fabrication of the micromachined sensor for use with nonadherent cells is to grow a 1-μm-thick SiO_2 layer by steam oxidation, followed by photolithographic patterning to form openings where the cavities will be located. The cavities are then anisotropically etched in an SF_6-C_2ClF_5 plasma, as described by Zdeblick *et al.* (*4*), producing cavities with walls at an angle of >85° from the horizontal. The final steps in the process are the growth of the thin oxide and the nitride deposition, as in the unpatterned case. The micromachined sensors thus have a thick oxide layer on the areas between cavities, effectively deactivating the sensing capability there. The active sensing surfaces are only the walls and floor of the cavities, improving the signal-to-noise performance.

The LAPS device detects the surface potential at illuminated regions of the interface between the electrolyte and the Si_3N_4 insulator. The presence of protonatable silanol and amine groups on this surface ensures that this potential depends on *p*H in a Nernstian fashion (*5*). In one version of the apparatus, the chamber is mounted on a microscope stage and the beam from a 10-mW HeNe laser is projected through the epi-illumination system onto the sensor, which allows flexibility in the position, shape, and area illuminated. In a second version no laser or microscope is used; instead, four separate and fixed sites, each ~1 mm^2, are probed from beneath the sensor by optic fibers connected to infrared light–emitting diodes. This is less flexible than the laser version, but is more economical and allows the simultaneous collection of data from multiple sites. Given that the density of a confluent monolayer of eukaryotic cells is ~10^5/cm^2, at each illuminated site information is obtained from ~10^3 cells in ~100 nl of medium.

There are three electrical connections to the chamber: (i) an platinum ribbon in contact with the indium–tin oxide controlling electrode; (ii) an Ag-AgCl reference electrode in an external well that measures the potential of solution in the flow chamber through a salt bridge which forms the chamber's outlet tube; and (iii) an ohmic connection to the base of the LAPS chip. A personal computer with a custom circuit board handles the acquisition, analysis, and display of data.

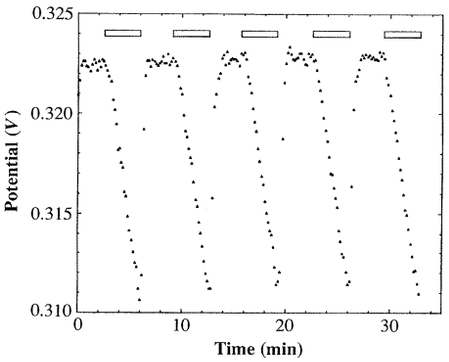

Fig. 2. Repetitive measurements of acidification rates. The figure shows sensor signal versus time for normal human keratinocytes (*29*) grown on a glass cover slip. The sensor flat-band voltage is linearly related to *p*H: a decrease of 61 mV is equivalent to an acidification by 1 *p*H unit. When the flow is on, the sensor measures a steady-state *p*H near that of the infusing medium. When it is off, during the periods denoted with bars, the cells acidify the medium. A linear least-squares fit to the rate of acidification is taken as a measure of the metabolic rate of the cells. The resumption of flow resets the *p*H for subsequent measurements. Cellular metabolic rates are determined once for every on-off cycle, which typically takes 5 to 7 min. The periods with flow off usually last 2 to 3 min, during which time the *p*H of the medium in the chamber drops 0.1 to 0.3 *p*H units. The acidification rate (± SE) from the five measurements depicted is −60 ± 2 μV/s or 0.06 ± 0.002 *p*H units/min.

The flow of culture medium, typically 10 to 100 μl/min, is provided by a syringe or peristaltic pump, again under computer control. Before entering the chamber, the medium passes through a degassing unit made of thin-walled silicone rubber tubing in a chamber maintained at about 2/3 atmospheric pressure. This procedure removes sufficient air from the medium to keep it from outgassing when it is warmed to 37°C in the temperature-regulated flow chamber.

Depending on the experiment, valves can be used to switch between different fluid streams or add boluses of test compounds through an injection loop. Normal cell-culture medium is used, including serum if desired, except that bicarbonate and buffers such as Hepes are excluded. Reducing the buffer capacity of the medium to ~1 m*M* increases the *p*H change of the medium for a given excretion of acid by the cells. Since the medium is in a closed system, no drift in *p*H occurs because of equilibration with atmospheric CO_2.

Metabolic rates are measured by determining acidification rates during periodic interruptions of the flow of medium through the flow chamber (Fig. 2). For the types of mammalian cells discussed in this paper, a confluent monolayer (equivalent to about 10^7 cells per milliliter) commonly produces acidification rates within a factor

of 2 of 100 μV/s. At 61 mV per *p*H and medium buffer capacity of 1 m*M*, this corresponds to a calculated net rate of H^+ production of $\sim 1 \times 10^8$ per second for a typical cell. The metabolic sources of these protons depend on the nutrients in the culture medium and the metabolic pathways that are active in the cells. Some insight into this can be gained with auxiliary biochemical measurements and specific metabolic poisons.

Oxygen consumption was measured in a separate perfusion apparatus equipped with a Clark O_2 electrode. The removal of O_2 from the media by a monolayer of the murine fibroblastic L cell line (*6*) was measured in the output stream under conditions of constant flow. Lactate production was also measured, with a spectrophotometric enzymatic assay based on the reduction of nicotinamide adenine dinucleotide (NAD^+). When culture medium was used as the bathing medium, the rates of O_2 consumption (approximating CO_2 production) and lactate production per cell (± SE, $n = 3$) were roughly equal at 3.1 (± 0.5) × 10^7 per second and 3.3 (± 0.3) × 10^7 per second. Similar results were obtained when the cells were tested in a balanced salt solution with 5 m*M* glucose as the only carbon source. Other cell types tested, for example CHO (*7*), were more heavily glycolytic.

The metabolic poison carbonylcyanide chlorophenylhydrazone (CCCP) is a respiratory uncoupler that stimulates mitochondrial oxygen uptake (*8*). The effect of 20 μ*M* CCCP on the nonadherent murine macrophage-like line P388D$_1$ is shown in Fig. 3A. The stimulation is prompt, faster than the resolution of the apparatus. It is reversible, with a recovery time of about 20 min after the removal of the uncoupler. Dose-response experiments show a maximum stimulation of the acidification rate near 2 to 5 μ*M* CCCP. Presumably the mechanism is a combination of increased CO_2 production and the stimulation of glycolysis to maintain homeostasis.

We have studied the response of normal human epidermal keratinocytes to epidermal growth factor (EGF), a substance found to be mitogenic for these cells (*9*) and included in their culture medium at 10 ng/ml. After EGF starvation for 24 hours, a rise in metabolic rate is evident within 5 min after the introduction of 50 ng/ml EGF to keratinocytes in the silicon microphysiometer (Fig. 3B). At the peak of the response, in ~15 min, the metabolic rate has nearly doubled; in another 15 min it has decayed to a steadily rising baseline. A parallel control experiment with a sham change of EGF-free medium (Fig. 3B) displays none of this biphasic behavior. It does show the same rising baseline, which probably indicates some combination of cell proliferation and adaptation to the environmental conditions in the flow chamber. Stimulation of acidification rate is observable down to 0.1 ng of EGF per milliliter. In a control experiment, the stimulation was abolished by a monoclonal antibody to EGF that is known to block receptor binding. These experiments demonstrate the ability of the biosensor to detect a cellular response to ligand-receptor binding on a time scale of minutes.

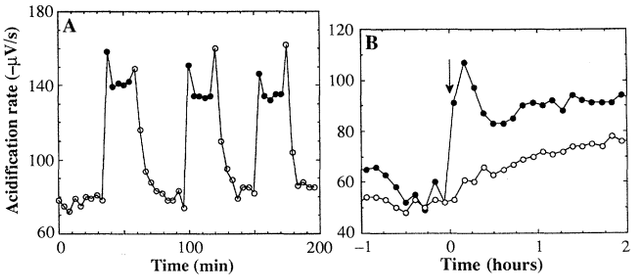

Fig. 3. (**A**) Response of P388D$_1$ cells to repeated applications of the metabolic uncoupler CCCP. ○, Control medium; ●, 20 μ*M* CCCP. This concentration increases rates less than does the optimum dose of 2 to 5 μ*M*, and the rate maxima at the beginnings of application and washout of CCCP reflect transient concentrations closer to that optimum. (**B**) Response of normal human keratinocytes to EGF. The normal culture medium contains EGF as well as an undefined component, bovine pituitary extract. Both were withheld from keratinocytes plated on cover slips for 24 hours before the experiment. The cells were mounted in two microphysiometer chambers under the same culture conditions, and at time 0 (arrow) EGF (50 ng/ml) was introduced into the medium of one chamber; ●, 50 ng of EGF per milliliter; ○, control (no EGF).

This effect of EGF on keratinocytes closely parallels that previously reported for mouse and human fibroblasts, where stimulation with EGF has been shown to lead to a rapid increase in glycolytic rate (*10*). The enhancement has been attributed to increased 6-phosphofructo-1-kinase activity as a result of increased concentrations of fructose-2,6-bisphosphate, a potent stimulator of the enzyme (*10, 11*). Fructose-2,6-bisphosphate has also been shown (*12*) to affect the stimulation of glycolysis in fibroblasts by serum, insulin, and phorbol esters. Modulation of glycolytic rates in response to hormonal activation has been reported in other cell types (*12*), including muscle and liver cells, thus lending support to the measurement of metabolic activity as a means of detecting hormonal stimulation.

The cytotoxic effects of chemotherapeutic drugs on tumor cell lines are commonly determined by assays that detect proliferation. We have performed cytotoxicity assays in the silicon microphysiometer using a previously characterized cellular system (*13*). MES-SA is a human uterine sarcoma line that is sensitive to doxorubicin and vincristine. The Dx5 line, derived by selection with doxorubicin from MES-SA, is resistant to these drugs by virtue of enhanced activity of the P-glycoprotein transporter, which confers multidrug resistance (*14*).

Experiments with the silicon microphysiometer reproduce these results with relatively few cells and no extended cell growth. At therapeutic doses of doxorubicin (1 μ*M*), the differential cytotoxicity in the two lines is maintained. Decreased acidification rates are evident at 15 hours for MES-SA, but not by 50 hours for Dx5 (Fig. 4A). At high (100 μ*M*) doses of the drugs, similar but more rapid results occur: cytotoxicity of doxorubicin is manifest by 0.5 hours for MES-SA and 2.5 hours for Dx5. The results for 100 μ*M* vincristine are 5 hours and 10 hours, respectively (Fig. 4B).

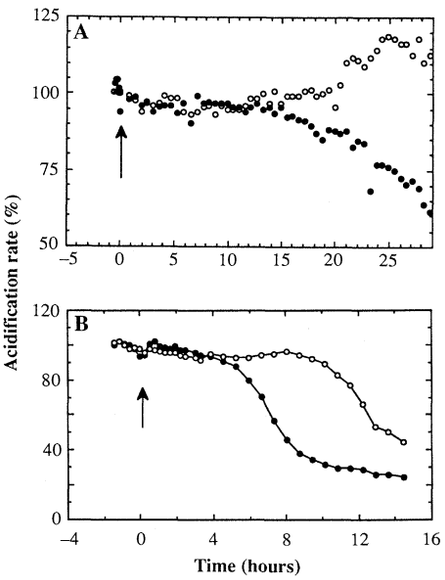

Fig. 4. Cytotoxicity of two chemotherapeutic drugs to sensitive and resistant tumor cell lines. Acidification rates are presented as percent of control rate before the drug was added to the culture medium that perfused the cells on the silicon microphysiometer at time 0 (arrow). Compared to the MES-SA cells (●), the Dx5 cells (○) are resistant to 1 μ*M* doxorubicin (**A**) and 100 μ*M* vincristine (**B**).

The complexity of the interactions involved in toxic effects makes the replacement of in vivo toxicological testing with in vitro methods extremely difficult. Nevertheless, there is measurable progress toward finding an in vitro replacement for the Draize (*15*) (rabbit eye) test for ocular irritancy. One strategy is to test the inhibitory effect of

Table 1. Comparison of the in vivo ocular irritancy (*28*) and MRD_{50} (volume fraction of irritant sufficient to reduce keratinocyte acidification rate by 50%). The irritancy testing protocol was to expose the cells to irritant for 5 min, wash the irritant away, and immediately determine the metabolic rate. Half-log serial dilutions of an irritant in culture medium were administered successively to a sample of cells, starting with the most dilute sample. The MRD_{50} was determined by interpolating a plot of acidification rate versus $\log_{10}$ (concentration). Reproducibility of the MRD_{50} data was within a factor of 2 (within 0.3 for the logarithm) over a period of months with different batches of cells.

Irritant	In vivo irritancy	$-\log_{10}(MRD_{50})$
Dimethyl sulfoxide	Mild	0.1
Propylene glycol	Mild	0.5
Methanol	Moderate to mild	0.7
Ethanol	Moderate to mild	0.8
Acetone	Moderate to mild	0.9
n-Butanol	Moderate	1.7
Na dodecyl sulfate	Severe to moderate	3.9
Benzalkonium Cl	Severe	4.1

compounds on the acidification of culture medium bathing cells in microtiter-plate wells (*16*). The incubation lasts up to 7 days and is primarily an assay for proliferation and cell death. Using the silicon microphysiometer, we have studied metabolic effects of irritants on a time scale of minutes, which is closer to the typical human exposure time.

For a panel of eight previously studied ocular irritants, we have determined the concentration of irritant sufficient to depress the metabolic rates of human keratinocytes by 50% after a 5-min exposure, the MRD_{50}. A high correlation between the ranking of these concentrations and the in vivo severity of the irritants is shown in Table 1. There is additional information in the tests. The duration (as well as severity) of toxic effects is important, and we have investigated the kinetics of recovery from exposure to irritant. For example, complete recovery from a single dose of dimethyl sulfoxide at the MRD_{50} was seen within 1 to 2 hours, but ethanol proved lethal within the same period. The concentration dependence of the response can also be complicated: some irritants increased acidification rates at slightly subinhibitory concentrations. Further analysis of such effects may lead to more insight into mechanisms of toxicity.

With the microphysiometer, a biological rather than a chemical agent can be used to interfere with cellular function. Vesicular stomatitis virus (VSV) is a cattle pathogen that can infect the murine fibroblastic L cell line. When grown aseptically in the silicon microphysiometer, L cells show a steady increase in acidification rates caused by proliferation. Exposure to VSV (*17*) has a prompt and a delayed effect. Within 2 hours of infection at multiplicities of infection (MOI) of greater than one virion per cell, the increase in acidification rate is diminished or abolished. Then, after a lag that depends on the MOI, a sharp decrease in acidification rate occurs at the onset of visually observable cytopathic effects (15, 12, and 8 hours for MOIs of 0.1, 1, and 10, respectively). There is no evidence of dramatic increases in metabolic rates because of the mobilization of the cells' metabolic systems for the production of virions.

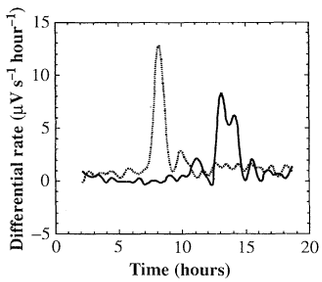

Fig. 5. Ribavirin inhibits the cytopathic effects of VSV infection on L cells. Here we have presented the data as the rate of change of acidification rate (control − infected) with respect to time, which produces positive peaks during periods of rapid decrease of the acidification rates of infected cells. At time 0, cells on cover slips in two microphysiometer chambers were exposed to VSV at MOI = 10. The medium contained either 200 μ*M* ribavirin (solid line) or no drug (dotted line).Uninfected cells in two additional chambers served as controls, with and without ribavirin. Under these conditions, the effects of ribavirin alone on acidification rates were small.

The cytopathic effects of VSV infection that we detect can be inhibited by the broad-spectrum antiviral agent ribavirin (*18*) (Fig. 5). In the absence of ribavirin, the precipitous decrease in cellular metabolism occurred about 8 hours after infection (at MOI = 10), but 200 μ*M* drug delayed the onset until 13 hours. A dose of 20 μ*M* ribavirin gave results indistinguishable from the 0 μ*M* control. At a lower MOI (= 1) the onset of cytopathic effects was not observed in the presence of 200 μ*M* ribavirin by 20 hours.

Complementary measures of cellular catabolic activity include the rates of consumption of glucose and O_2, as well as the rates of production of lactate, CO_2, and heat. Of these, the best developed methods relevant to the present work are oximetry with the Clark O_2 electrode (*19*) and microcalorimetry (*20*). The flux of metabolites can also be determined by nuclear magnetic resonance spectroscopy (*21*). Differentiating features of the silicon microphysiometer include spatial resolution (~1 mm) and the small number of cells required (~10^3). The fluidics system is adapted both to rapid (seconds) composition changes in the medium and to long-term culture (we have kept cells alive in the chamber under continual analysis for as long as 90 hours). Both adherent and nonadherent cells can be analyzed with minimal perturbations. A limitation is the requirement for low-buffered medium (low bicarbonate content) to achieve maximum sensitivity.

Previous applications of silicon technology to cell biology have included the growth of neurons on chemically patterned (silanized) substrates (*22*) and the connection of neurons in vitro to silicon-based microelectrodes (*23*). The metabolic applications we have presented have exploited only a small portion of what is achievable with silicon biosensor technology. For example, state-of-the-art silicon technology routinely is used to fabricate structures with feature sizes in the 1-μm range, including deep trenches (*24*). Fluidics components such as valves and micropumps have also been made on silicon wafers (*25*). The combination of all these elements permits us to envision devices involving many parallel channels, in which a few cells are exposed to compounds under study and where the fluidics are integrated with the metabolic sensors. Whether it ultimately will be practical to analyze single cells will depend more on improvements in sensor sensitivity than on micromechanical issues.

We anticipate that this silicon microphysiometer will be particularly useful for screening for new therapeutic drugs, and also for toxicology. In both areas one seeks cellular clues, sometimes subtle, weak, or transient, indicating that a chemical substance affects the biochemical state of cells. Once these clues are found, the more traditional pharmacological, chemical, and toxicological techniques can then be used. Potential applications for the technique in cancer pharmacology include the identification of new cytotoxic compounds, drug-sensitivity testing of tumor cells, and studies of variations in drug sequence and scheduling in combination chemotherapy. Investigators can use cells in the microphysiometer to detect biochemicals (by analogy to the work of Karube (*26*), Rechnitz (*27*), and others), viruses, and products released by one cell that affect a second cell.

REFERENCES AND NOTES

1. D. G. Hafeman, J. W. Parce, H. M. McConnell, *Science* **240**, 1182 (1988).

2. K. Nilsson, *Trends Biotechnol.* **5**, 73 (1987).
3. The hydrodynamics for such geometries, termed separated flow, is fairly well understood [R. F. Weiss and B. H. Florsheim, *Phys. Fluids* **8**, 1631 (1965)]. At creeping flow rates (our low flow–rate regime) a vortex circulates within the well so that none of the streamlines in the bulk fluid penetrate deeply into the well; mass transport between the well and the bulk fluid is diffusive across a flow boundary near the mouth of the well. We have observed the circulation of cells within such vortices. An array of trenches 50 μm wide by 1 mm long by 50 μm deep, separated by 25-μm walls and oriented normal to the flow direction, also works well.
4. M. J. Zdeblick, P. P. Barth, J. B. Angell, *Sensors Actuators* **15**, 427 (1988).
5. D. L. Harame, L. J. Bousse, J. D. Meindl, *IEEE Trans. Electron Devices* **34**, 1700 (1987).
6. The cells were obtained from A. Waitz and were maintained in Dulbecco's modified Eagle's medium with 10% fetal bovine serum. Unless otherwise noted, this medium was used for all cells studied here.
7. CHO cells were obtained from American Type Culture Collection, as were all other cells unless otherwise noted.
8. E. C. Weinbach and P. S. Ebert, *Cancer Lett.* **26**, 253 (1985).
9. G. D. Shipley and M. R. Pittelkow, *Arch. Dermatol.* **123**, 1541a (1987).
10. I. Diamond, A. Legg, J. A. Schneider, E. Rozengurt, *J. Biol. Chem.* **253**, 866 (1978).
11. M. Farnararo, V. Vasta, P. Bruni, A. D'Alessandro, *FEBS Lett.* **171**, 117 (1984).
12. L. Hue and M. H. Rider, *Biochem. J.* **245**, 313 (1987).
13. W. G. Harker and B. I. Sikic, *Cancer Res.* **45**, 4091 (1985).
14. G. Bradley, P. F. Juranka, V. Ling, *Biochim. Biophys. Acta* **948**, 87 (1988).
15. J. H. Draize, G. Woodard, H. O. Calvery, *J. Pharmacol. Exp. Ther.* **82**, 377 (1944); J. F. Griffith *et al.*, *Toxicol. Appl. Pharmacol.* **55**, 501 (1980).
16. J. Selling and B. Ekwall, *Xenobiotica* **15**, 713 (1985); for related work see D. G. Wenzel and G. N. Cosma, *Toxicology* **29**, 173 (1983).
17. The virus (Indiana strain) was obtained from D. Lyles.
18. R. W. Sidwell *et al.*, *Science* **177**, 705 (1972).
19. I. Karube, T. Matsunaga, S. Suzuki, *Anal. Chim. Acta* **109**, 39 (1979); X-M. Li, B. S. Liang, H. Y. Wang, *Biotechnol. Bioeng.* **31**, 250 (1988).
20. A. M. James, Ed., *Thermal and Energetic Studies of Cellular Biological Systems* (Wright, Bristol, 1987).
21. R. S. Balaban, *Am. J. Physiol.* **246**, C10 (1984); S. L. Campbell-Burk, J. A. den Hollander, J. R. Alger, R. G. Shulman, *Biochemistry* **26**, 7493 (1987).
22. D. Kleinfeld, K. H. Kahler, P. E. Hockberger, *J. Neurosci.* **8**, 4098 (1988).
23. W. G. Regehr, J. Pine, D. B. Rutledge, *IEEE Trans. Biomed. Eng.* **35**, 1023 (1988).
24. M. Engelhardt and S. Schwarzl, *J. Electrochem. Soc.* **143**, 1985 (1987).
25. H. T. G. van Lintel, F. C. M. van de Pol, S. Bouwstra, *Sensors Actuators* **15**, 153 (1988); M. J. Zdeblick and J. B. Angell, *Digest of the 4th International Conference on Sensors and Actuators* (Institute of Electrical Engineers of Japan, Tokyo, Japan, 1987), pp. 827–829.
26. I. Karube, in *Biosensors: Fundamentals and Applications*, A. Turner, I. Karube, G. Wilson, Eds. (Oxford Univ. Press, Oxford, 1987), chap. 2.
27. M. Arnold and G. Rechnitz, *ibid.*, chap. 3.
28. C. Shopsis, E. Borenfreund, J. Walberg, D. M. Stark, *Food Chem. Toxicol.* **23**, 259 (1985). These authors compiled the in vivo irritancy assessments from an analysis of published data in sources such as W. M. Grant, *Toxicology of the Eye* (Thomas, Springfield, IL, ed. 2, 1974); and G. Clayton and F. Clayton, Eds., *Patty's Industrial Hygiene and Toxicology* (Wiley, New York, ed. 3, 1982).
29. The adherent cells and medium were obtained from Clonetics. The KGM medium is essentially the same as that described in S. T. Boyce and R. G. Ham, *J. Tissue Cult. Methods* **9**, 83 (1985). The cells were morphologically undifferentiated visually and were used at 80 to 90% confluence.
30. We gratefully acknowledge engineering assistance from J. Kercso and G. Pontis, and technical assistance from F. Butt. Supported in part by the U.S. Army CRDEC and DARPA programs, ARO contract DAAL03-86-C-0009 to M.D.C., and NIH grant R01-CA-4217 and the American Cancer Society grant CH-411 to B.I.S.

6 June 1989; accepted 16 August 1989

One Enzyme Makes a Fungal Pathogen, But Not a Saprophyte, Virulent on a New Host Plant

W. SCHÄFER,* D. STRANEY,† L. CIUFFETTI, H. D. VAN ETTEN,‡ O. C. YODER

Certain genes of *Nectria haematococca*, a fungal pathogen of pea (*Pisum sativum*), encode pisatin demethylase (pda), a cytochrome P-450 monoxygenase that detoxifies the phytoalexin pisatin. Because pda is required by *N. haematococca* for pathogenicity on pea, pisatin helps defend pea against *N. haematococca*. The possibility that pisatin is a general defense factor—that is, that pda can confer pathogenicity to fungi not normally pathogenic on pea—was investigated. Genes encoding pda were transformed into and highly expressed in *Cochliobolus heterostrophus*, a fungal pathogen of maize but not of pea, and in *Aspergillus nidulans*, a saprophytic fungus, neither of which produces a significant amount of pda. Transformants contained at least as much pda as did wild-type *N. haematococca*. Recombinant *C. heterostrophus* was normally virulent on maize, but it also caused symptoms on pea, whereas recombinant *A. nidulans* did not affect pea. Thus, phytoalexins can function in nonspecific resistance of plants to microbes; saprophytes appear to lack genes for basic pathogenicity.

ONE HYPOTHESIS CONCERNING the cause of plant disease is that the successful pathogen can prevent or disarm plant defenses. Among the best known plant responses to a stress such as microbial attack is the synthesis of antimicrobial secondary metabolites called phytoalexins. Fungal detoxification of a plant's phytoalexins has been suggested as a general mechanism for circumventing phytoalexin-mediated plant defense (*1*).

The filamentous ascomycete *Nectria haematococca* Berk. and Br. mating population VI (anamorph: *Fusarium solani*) is a pathogen of pea and uses the detoxification strategy, since it can degrade the pea phytoalexin pisatin to a less toxic compound (*1*). This detoxifying activity is due to a substrate-inducible cytochrome P-450 monoxygenase called pisatin demethylase (pda). Data, based on analyses of progenies in which Pda is segregating, confirm that pda is necessary for pathogenicity (*1*). Moreover, when a cloned gene (*PDA-T9*) encoding pda (*2*) is transformed into a nonpathogenic Pda^- strain of *N. haematococca*, the recombinant strain can attack pea (*3*). These results indicate that pda is required by *N. haematococca* for pathogenicity on pea and that pisatin itself is a plant defense factor.

We designed experiments to assess the role of pisatin in defense of pea against fungi not normally pathogenic to pea. Genes encoding pda (*2, 4–8*) were transformed (*7–10*) into *Cochliobolus heterostrophus*, a pathogen of maize but not pea, and *Aspergillus nidulans*, a saprophyte, by means of vectors (*4–8*) and strains (*11–14*) designed for this purpose. To achieve overexpression of pda, we chose transformants with high copy numbers of the transforming plasmid in their genomes (*15–17*). A *C. heterostrophus* transformant (strain C2-P) and an *A. nidulans* transformant (strain UCD1-P), which carried 18 and 12 copies of the transforming plasmid (*16, 18, 19*), respectively, were used for further experiments. Control *C. heterostrophus* transformant C2-V and *A. nidulans* transformant UCD1-V each contained comparable numbers of the respective vectors alone (*15–17*).

Rates of pisatin demethylation by transformants C2-P and UCD1-P were equal to or greater than those of the highly virulent, rapidly demethylating *N. haematococca* wild-type strain N77-2-3 (Figs. 1 and 2). Strains C2, C2-V, UCD1, and UCD1-V had background pda levels 0 to 7% of those of

Department of Plant Pathology, Cornell University, Ithaca, NY 14853.

*Present address: Institut fur Genbiologische Forschung Berlin GmbH, Ihnestrasse 63, 1000 Berlin 33, Federal Republic of Germany.
†Present address: Department of Botany, University of Maryland, College Park, MD 20742.
‡Present address: Departments of Plant Pathology and Molecular and Cellular Biology, University of Arizona, Tucson, AZ 85721.